MDPI

Article

Enhancement of the NORAD-Atomic-Data Database in Plasma

Sultana N. Nahar [1,*,†] and **Guillermo Hinojosa-Aguirre** [2,†]

1   Department of Astronomy, The Ohio State University, Columbus, OH 43210, USA
2   Instituto de Ciencias Físicas, Universidad Nacional Autónoma de México, A. P. 48-3, Cuernavaca 62251, Mexico; hinojosa@icf.unam.mx
*   Correspondence: nahar.1@osu.edu; Tel.: +1-614-292-1888
†   These authors contributed equally to this work.

Abstract: We report recent enhancements to the online atomic database at the Ohio State University, NORAD-Atomic-Data, that provide various parameters for radiative and collisional atomic processes dominant in astrophysical plasma. NORAD stands for Nahar Osu RADiative. The database belongs to the data sources, especially for the latest works, of the international collaborations of the Opacity Project and the Iron Project. The contents of the database are calculated values for energies, oscillator strengths, radiative decay rates, lifetimes, cross-sections for photoionization, electron-ion recombination cross-sections, and recombination rate coefficients. We have recently expanded NORAD-Atomic-Data with several enhancements over those reported earlier. They are as follows: (i) We continue to add energy levels, transition parameters, cross-sections, and recombination rates for atoms and ions with their publications. (ii) Recently added radiative atomic data contain a significant amount of transition data for photo-absorption spectral features corresponding to the X-ray resonance fluorescence effect, showing prominent wavelength regions of bio-signature elements, such as phosphorus ions, and emission bumps of heavy elements, such as of lanthanides, which may be created in a kilonova event. We are including (iii) collisional data for electron-impact-excitation, (iv) experimental data for energies and oscillator strengths for line formation, (v) experimental cross-sections for photoionization that can be applied for benchmarking and other applications, and (vi) the introduction of a web-based interactive feature to calculate spectral line ratios at various plasma temperature and density diagnostics, starting with our recently published data for P II. We presented a summary description of theoretical backgrounds for the computed data in the earlier paper. With the introduction of experimental results in the new version of NORAD, we present a summary description of measurement of high-resolution photoionization cross-sections at an Advanced Light Source of LBNL synchrotron set-up and briefly discuss other set-ups. These additions should make NORAD-Atomic-Data more versatile for various applications. For brevity, we provide information on the extensions and avoid repetition of data description of the original paper.

Keywords: atomic data; transition probabilities; photoionization cross-sections; electron-ion recombination cross-sections and rate coefficients; lifetimes; electron-impact excitation; line ratios; third-generation synchrotron radiation for photoionization

1. Introduction: NORAD-Atomic-Data

The atomic database, NORAD-Atomic-Data [1,2], contains parameters of atomic processes, as described below, that are dominant in astrophysical plasma. A major part of the data was obtained under the two international collaborations of the Opacity Project (OP) [3,4] and the Iron Project (IP) [5], and constitute the atomic data source, either for new data or revised and expanded data for the OP and the IP.

The author (SNN) is the leading member of the Opacity Project ([4]) and the Iron Project (IP [5]) for studying the radiative atomic processes and has been computing extensive sets of radiative data. To meet the need of astronomers to access atomic data at all times from an independent platform, the online database NORAD-Atomic-Data [1,2] was founded in 2007

at the Ohio State University. NORAD-Atomic-Data provides data that are not available or that are updated with larger wavefunction expansion and higher accuracy than those in the two atomic databases, TOPbase [6] founded under the OP and TIPbase [7] founded under the IP. All data are processed for clarity and easy applications before uploading them to NORAD-Atomic-Data as explained in [1]. This report presents several recently added enhancements and those under development in the latest form of the database.

Details of format and data structure, a summary of theoretical background, and an accuracy estimation of data for the processes have been described in Nahar [1]. A more detailed theoretical background is available from the textbook of Pradhan and Nahar Atomic Astrophysics and Spectroscopy (AAS11) (Cambridge University press, 2011) [8], which is a culmination of findings in atomic processes revealed in the study under the OP and IP. For the new additions of experimental data in NORAD-Atomic-Data, we present summary outlines for experimental methods and more details of one particular experimental method with an Advanced Light Source (ALS) at Lawrence Berkeley National Laboratory (LBNL) synchrotron, which provides high-resolution photoionization cross-sections.

We provide outlines below for general guidance on the atomic processes in plasma and relevant contents of the database.

2. Atomic Processes and Parameters in NORAD-Atomic-Data

There are four atomic processes that occur commonly in astrophysical plasma: photo-excitation, photoionization, electron–ion recombination, and electron-impact excitation. The study of an atomic process requires wavefunctions and energy levels of the atomic system being studied to calculate various parameters of the processes. These parameters, available in the NORAD-Atomic-Data database, have been computed using energy levels and wavefunctions generated either by the R-matrix method using its package of, and associated, codes [9,10] along with spectroscopy codes ELEVID [11], and PRCBPID [12], or by central-field approximation using atomic structure code SUPERSTRUCTURE (SS) [13,14]. The following are the atomic processes and associated data files.

(i)   Energy levels

NORAD-Atomic-Data provides energy tables for each atomic species for which atomic processes have been studied. Although basically the same, there are some differences in representations between the energies obtained from the R-matrix method and from atomic structure calculations.

The R-matrix method calculates absolute values for the energy levels and can show the clear presence of an ionization threshold as negative energies for bound levels turn positive for continuum levels when energies reach the threshold. This option is enabled in the R-matrix codes for nonrelativistic LS coupling approximation [9]. The latest version of the relativistic Breit–Pauli R-matrix (BPRM) codes [10] computes only the bound levels, that is, no positive energies are computed. In contrast to R-matrix, SS computes energy values relative to the ground level, which is set to zero, and hence shows positive values. This representation is the same as that for energies compiled and available on the website of the National Institute of Standards and Technology (NIST [15]). Atomic structure calculations, such as SS, do not determine the ionization threshold and compute all energy levels belonging to the set of configurations provided. Hence, the computed energies can continue from bound to beyond the ionization threshold. The NIST provides ionization thresholds that have been obtained separately.

Energy levels computed in the R-matrix method [9,10] go from ground level to highly excited levels with $n \leq 10$, $l \leq 9$, and of parities even and odd, and hence correspond to a large set of levels. The number of energy levels from SS [13,14] is typically less since the excitation goes up to $n \leq 4$–6, although it includes all possible energies from combinations of configurations.

R-matrix computations include all quantities, such as oscillator strengths, photoionization cross-sections, and electron–ion recombination rate coefficients for all levels going up

to $n = 10$. SS computes all transition parameters for levels going up to the highest orbitals with $n = 4$–6.

Formats for the energy files are described in [1].

(ii) Radiative atomic transition of excitation and de-excitation

$$X^{+q} + h\nu \rightleftharpoons X^{+q*} \tag{1}$$

X^{+q} is the ion of X of charge q and an asterisk indicates excitation. The parameters of interest are (i) line strength (S), (ii) oscillator strength (f), (iii) radiative decay rate (A-value) for the transitions, and (iv) lifetimes (τ) of levels.

Radiative data for bound–bound transitions are of the following types: allowed electric dipole (E1) of the same spin (for *LS*-allowed and fine structure) and different (intercombination) spin multiplicities of the final state from the initial one, electric quadrupole (E2), electric octupole (E3), magnetic dipole (M1), and magnetic quadrupole (M2). Details of these are described in [8]. For many ions in the database, E1 transitions have been obtained from the BPRM method, while parameters for forbidden transitions have been obtained from Breit–Pauli atomic structure calculations using code SS. When the R-matrix method has not been used, E1 transitions obtained using SS are presented. Individual transitions form spectral lines. However, data for a large number of transitions are needed to determine the opacity in plasma, creation of synthetic spectrum of ions, etc.

Formats for the transition parameters are described in [1].

(iii) Photoionization (PI)

The process proceeds directly by photoabsorption as

$$X^{+q} + h\nu \rightarrow X^{+q+1} + e \tag{2}$$

which produces a smooth photoionization cross-section (σ_{PI}) feature, such as the background σ_{PI}. Photoionization can occur indirectly via formation of an intermediate doubly excited autoionizing state before ionization as

$$h\nu + X^{+q} \rightleftharpoons (X^{+q})^{**} \rightleftharpoons X^{+q+1} + e \tag{3}$$
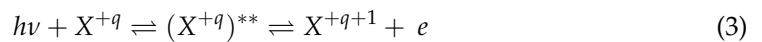
This takes place when the photon energy matches that of a Rydberg state and introduces a resonance, known as a Rydberg resonance, in the cross-section σ_{PI}. A resonance has considerable impact, not only by its magnitude of very high probability, but also on the shape of the background cross-section. In addition to Rydberg series of resonances, a Seaton resonance also forms when the core ion goes through a dipole-allowed transition before breaking down for photoionization (explained in, i.e., in AAS11).

Central-field approximation, such as distorted wave, produces only the background photoionization cross-sections, not the resonances. Only the close-coupling (CC) approximation using the R-matrix method can produce resonances automatically along with background cross-sections. We use relativistic Breit–Pauli R-matrix (BPRM) codes [10] with a correction code [16] and use CC wavefunction expansion to compute σ_{PI}. The resonances are treated with a radiation damping effect [17] for precise treatment. However, we also use nonrelativistic R-matrix codes [9] when relativistic fine structure calculations become computationally prohibitive.

The parameters calculated for photoionization are the cross-sections for all bound levels from ground to $n \leq 10$. They are usually of two types: (i) partial cross-section for photoionization $\sigma_{PI}(g, E)$, leaving the core ion at its ground level and (ii) total cross-section for photoionization σ_{PI}, leaving the core ion in the ground and various excited states as the photon energy crosses the excitation thresholds. Total cross-section is the sum of all partial cross-sections leaving the core ion in various states. (iii) We also calculate the individual partial cross-sections, leaving the core ion at various excited levels. However, such partials are saved only for the ground level for which these cross-sections have more applications.

Formats for photoionization cross-sections are described in [1].

(iv) Electron–ion recombination

This is the inverse process of photoionization where electrons and ions can recombine directly, known as radiative recombination (RR), as

$$X^{+q+1} + e \rightarrow X^{+q} + h\nu, \tag{4}$$

This provides the smooth background feature of the recombination cross-section. Recombination can also occur through an intermediate recombination (DR), as

$$e + X^{+q} \rightleftharpoons (X^{+q-1})^{**} \rightleftharpoons \begin{cases} e + X^{+q} & \text{AI} \\ X^{+q-1} + h\nu & \text{DR} \end{cases} \tag{5}$$
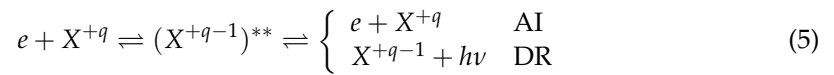
The intermediate autoionizing state can lead to autoionization (AI) where the electron goes free, or to radiative decay of DR by emission of a photon.

For electron–ion recombination, we calculate the atomic parameters using the unified method of Nahar and Pradhan [16,18] for (i) level-specific total recombination (includes both RR and DR) rate coefficients ($\alpha_{RC}(i)$) of all bound levels going up to $n \leq 10$; (ii) total recombination rate coefficient with respect to temperature $\alpha_{RC}(T)$), which is the summed contributions of all levels with $n \leq 10$ and of levels with $10 < n \leq \infty$ obtained using the extension of Nahar and Pradhan (1994) of Bell and Seaton theory [19] on DR; (iii) total recombination cross-sections ($\sigma_{RC}(E)$); and (iv) total recombination rate coefficient ($\alpha_{RC}(E)$) with respect to photo-electron energy E. Recombination resonances can be seen in emission spectra as dielectronic recombination (DES) lines and total $\alpha_{RC}(T)$ are used in the determination of ionization fractions in photoionized or collisional plasma. The data format is explained in [1].

(v) Electron-impact excitation (EIE)

Electron-impact excitation of a target leads to the emission of a photon as the excited electron drops down:

$$e + X^{+Z} \rightarrow e' + X^{+Z*} \rightarrow X^{+Z} + h\nu + e' \tag{6}$$
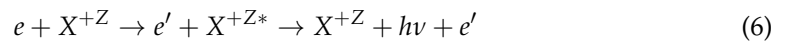
The line of the emitted photon carries information of the process. Similar to photoionization, an autoionizing state that introduces a resonance can form if the impact energy equals to that of a Rydberg state. EIE parameters are (i) collision strength (Ω), (ii) effective collision strengths (γ), and (iii) collision rate coefficients (q_{ij}). Emission lines from levels excited by EIE provide diagnostics of thin plasma. Details can be found in, e.g., in AAS11 [8].

3. Merged Beam Technique at the Advanced Light Source at the Lawrence Berkeley National Laboratory

For a general overview of the measurement of photoionization cross-sections, we provide a summary description of the experimental set-up that was installed at the Advanced Light Source (ALS) Synchrotron Facility at the LBNL. This is one of the most accurate experimental set-ups with third-generation synchrotron radiation for a high-resolution photoionization cross-section.

For a review of the merged beam technique (MBT), we refer to the article by Phaneuf et al. [20]. For more information about synchrotron technology, we refer to the article by Margaritondo [21]. For a detailed description of this experimental set-up, we refer to reference [22]. Here, we present a brief but complete description of the method.

To implement the experimental realization of photoionization Equation (2), an ion beam and a photon beam are merged. Also, parameters, such as their width, intensity, and overlap length have to be measured.

3.1. The Photon Beam

The experimental set-up was located at the ALS, a third-generation synchrotron accelerator at the LBNL. The Merged Beam Technique (MBT) was implemented in one of the end-lines of the synchrotron ring (beam line 10.0.1.). The end-station was intended to be a multi-user experiment. This MBT end-station was decommissioned in 2015 and by the end of the MBT operational time, the synchrotron's electron's storage ring operated with 500 mA current at 1.9 GeV in *top-off* mode, i.e., with a quasi-continuous injection of electrons that results in a constant current and stability improvement.

The photon beam was generated by a 10 cm period undulator inserted in the electron's trajectory inside the synchrotron's ring. As a result, the relativistic electrons oscillate producing a photon beam with a width of less than 1 mm and with a divergence less than $0.05°$. This photon beam was then directed to shine over a grazing spherical-grating monochromator, producing wavelength separation as a function of the grazing angle. In this manner, it was possible to scan the photon energy by rotating the grating. Also, the exit slit of the monochromator and the undulator gap were adjusted to maximize the photon beam intensity.

A calibrated silicon photodiode [23] with a 5% uncertainty was used to measure the photon flux. This diode generated a current that was read by a precision current meter that provided a normalization signal to the data acquisition system. Collisions of the X^{q+} ions with the residual gas in the vacuum system may generate $X^{(q+1)+}$ signal. To separate this background signal from the actual photoionization signal, the photon beam was mechanically pulsed using a controlled chopper-wheel to produce a signal correlated to photons and a signal correlated only to background $X^{(q+s)+}$, and in turn subtract it from the signal generated when the photons were on. s is the order of photoionization. For instance, $s = 1$ corresponds to single photoionization.

The energy resolution of the photon beam was typically between 10 meV and 40 meV and it was nominally programmed on the control system to later derive a more realistic value from full width half maximum (FWHM) of resonance peaks. The energy of the photon beam was nominally set by the control interface system associated to the beam line. The energy calibration was further improved with the aid of an ionization gas-cell located on a side branch of the experimental set-up; in this cell, He [24] and Kr [25] gases were injected. Their ionization spectra were used as a reference in the energy interval from 21.218 eV to 63.355 eV. Estimates of the energy error from this technique varied from about ± 30 meV to ± 10 meV, depending on different author's implementations. For instance, this calibration was employed for the single photoionization spectrum measurement of Cl^+ (see Table 1) resulting in an agreement with the NIST database [26] up to three decimal digits (in eV).

Although, the photon flux and resolution of this facility were uniquely fitted to measure photoionization, higher-order harmonic components in the photon beam, especially in the lower energy interval of its operational range (17 eV to 80 eV) can have considerable effects. This issue was assessed in references [22,23,27].

3.2. The Ion Beam

To generate the ion beam, an initial stage to create the ions was implemented by installing an ion source. Different types of ion sources were positioned in the end-station. For instance, an electron cyclotron resonance (ECR) ion source was used to generate multicharged ion beams. For example, C^{2+}, N^{3+}, and O^{4+} [28]. In the initial stage of the experiment, a hot-filament ion source was used to generate O^+ [29] and Ne^+ [30] ions; a caesium-sputter ion source was used for Na^- [31], and a plasma emission source produced Li^+ ions [32].

The ion source was mounted on a floated voltage circuit in a way that the whole ion source was biased to the acceleration voltage. As a consequence, ions generated inside the ion source were repelled or extracted by Coulomb repulsion. The standard repulsion

voltage was 5 kV or 6 kV to produce ion beams of energies of the order of keV because at these energies, the ionization by collision with the residual gas is expected to be low.

X^{q+} ions extracted from the ion source were accelerated toward a cylindrical electrostatic lens set that provided focusing to the ions. Following this, the ions were selected by mass-to-charge analysis with a 60° sector magnet. It is necessary to have fine control of the ion beam direction; for this purpose, sets of electric fields perpendicular to the ion beam trajectory were implemented by applying small voltages to steering plate electrodes (not shown in Figure 1) located at the entrance and the exit of a deflector made of two spherical-sector electrodes. This deflector produced a 90° change in the ion beam trajectory for the ion beam to face the counter-propagating photon beam from the ALS.
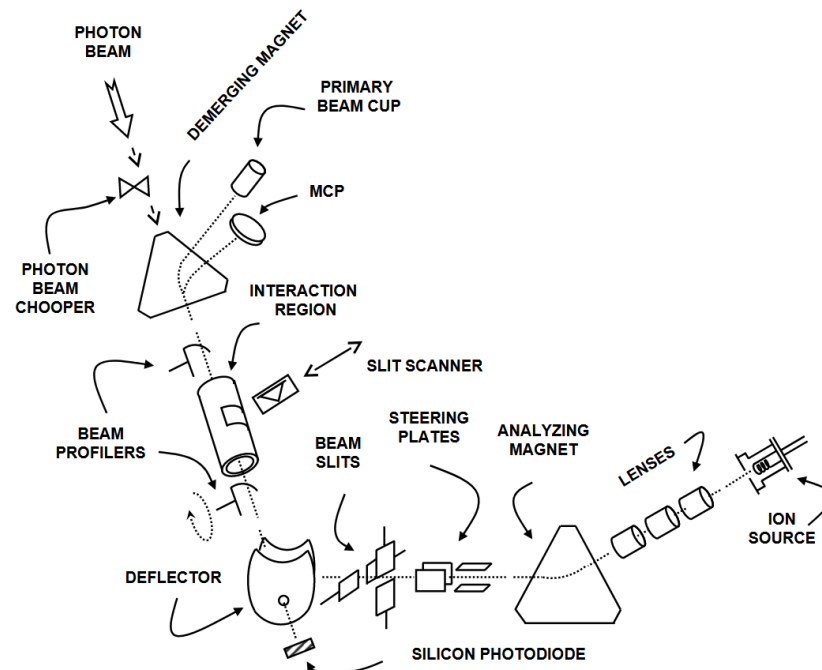
Figure 1. Schematic of the MBT end-station.

In this stage, the photon beam and the ion beam overlap, and as a consequence, photons can ionize the ion beam. Ions resulting from the overlapping will be called photo-ions. Photo-ions and the ion beam traveled through a voltage bias (typically, 2 kV) metallic mesh or interaction region. Photo-ions produced in this section suffer a different electric field from those photo-ions produced outside, thereby defining a fixed interaction distance. In this manner, photo-ions produced in this region had a different energy and it was possible to separate them from the parent ion beam by a second analyzing magnet. The interaction region has entrance and exit apertures to help define an effective interaction length. The experiment operated under ultrahigh vacuum conditions.

Intensity distributions $I(x, y)$ of both beams were measured by rotating-wire beam profilers installed before and after the interaction region. A third beam profiler consisted of a mechanically translating-slit scanner positioned halfway up the interaction region.

A second analyzing magnet separated the X^{q+} ion beam from the $X^{(q+s)+}$ photo-ions. The parent ion beam was monitored by an elongated Faraday cup. The second magnetic field was adjusted such that the $X^{(q+s)+}$ photo-ions passed through an aperture in the back of the Faraday cup. A spherical 90° electrostatic deflector directed them onto a stainless steel plate biased at -550 V, from which secondary electrons were accelerated and detected by a microsphere-plate electron multiplier used in a pulse-counting mode.

The detector's planes were perpendicular to the beam trajectory, allowing the photo-ions be scanned across the detector, and verify the full collection by measuring a plateau as a function of the pertinent parameters. The efficiency of the photo-ion detector was

calibrated in situ using an averaging sub-femtoampere meter to record the $X^{(q+s)+}$ photo-ion current, which was then compared to the measured photo-ion count rate. The primary X^{q+} ion beam current was measured by a precision current meter.

The overlap of the photon and ion beams, in addition to the interaction region dimensions, are needed to measure the cross-section. For this purpose, the beam intensity distributions measured with the beam profilers, $I^+(x,y)$ of the ion beam and $I^\gamma(x,y)$ of the photon beam, were measured, and a form factor $F(z)$ was derived according to

$$F_i(z) = \frac{\int \int I^+(x,y)I^\gamma(x,y)dxdy}{\int \int I^+(x,y)dxdy \int \int I^\gamma(x,y)dxdy} \, , \tag{7}$$

where z is the axis assigned to the propagation direction of the ion beam. $F(z)$ was sampled at the three positions where profilers were mounted: the entrance, the center, and the exit of the interaction region. These values, $F_i(z)$, were used to derive $F(z)$ by interpolation along the total interaction region length and derive, by integration over z, the spatial overlap of the photon and ion beams in the interaction region path.

The photoionization cross-section, σ, was derived from the experimental parameters as follows:

$$\sigma = \frac{Rqe^2 v_i \epsilon}{I^+ I^\gamma \int F(z)dz} \, , \tag{8}$$

where R is the photo-ion count rate, q is the charge state of X^{q+} parent-ion, $e = 1.6 \times 10^{-19}$ C, v_i is the ion beam velocity in cm $\cdot$ s^{-1}, ϵ is the responsivity of the photo-diode (electrons per photon), I^+ is the ion beam current (A), and I^γ is the photo-diode current (A).

3.3. Past Reviews on Measured Photoionization of Ions

We present a list of references for photoionization cross-sections for various ions measured at ALS in Table 1. We discuss cross-sections from other set-ups and the sources of information below.

There exist some reviews on the subject of earlier measurements of photoionization cross-sections. The review by Schmith in 1992 [33] presents a comprehensive treatment of both theory and experimentation with synchrotron radiation up to that date. There is still no reference to the merged beam technique. It is a handy reference for general aspects and terminology of first principles theoretical methods. The Sonntag and Zimmermann review in 1992 [34] concentrates on PI experiments of metallic vapors with synchrotron radiation above 20 eV. It presents an interesting review of available techniques to that date, like He-discharge and lasers. The authors mentioned that R-matrix is a more convenient method to describe PI over extended energy regions.

In West's 2001 review [35], it is mentioned that there were two main methods to measure photoionization spectra and cross-sections, plasma discharge and merged beam technique. He brings forward that the first experimental measurements of photoionization cross-sections were reported by Lyon and collaborators [36]. Up to the date of the review, the majority of measurements are concentrated in spectra measured with the plasma discharge method. A description of the plasma ionization technique evolution is presented. In this review, the merged beam technique is described to a good extent. This review emphasizes cases where both methods, plasma ionization and the merged beam technique, have been complementary. It raises the fact that the amount of experimental data available to date was not comparable with the data generated by theory; to a certain degree, this statement is still valid. By 2006, Kjeldsen [37] covered the state of the art, focusing on MBT experimentation with synchrotron radiation. Finally, the photoionization of metal atoms is also reviewed by [38] and PI data relevant to astrophysics are reviewed by Schippers and Müller [39].

Table 1. List of photoionization measurements of simple ions at the ALS with their references.

Photoionization			Reference
Li II	$\longrightarrow$	Li III	S. W. J. Scully, et al., J. Phys. B: At. Mol. Opt. Phys., **39**, 3957, 2006 [32] (https://iopscience.iop.org/article/10.1088/0953-4075/39/18/024, accessed on 13 December 2023)
B III	$\longrightarrow$	B IV	A. Müller, et al., J. Phys. B: At. Mol. Opt. Phys., **43**, 135602, 2010 [40] (https://iopscience.iop.org/article/10.1088/0953-4075/43/13/135602/meta, accessed on 13 December 2023)
B II	$\longrightarrow$	B III	S. Schippers, et al., J. Phys. B: At. Mol. Opt. Phys., **36**, 3371, 2003 [41] (https://iopscience.iop.org/article/10.1088/0953-4075/36/16/301/meta, accessed on 13 December 2023)
B II	$\longrightarrow$	B III	A. Müller, et al., J. Phys. B: At. Mol. Opt. Phys., **47**, 135201, 2014 [42] (https://iopscience.iop.org/article/10.1088/0953-4075/47/13/135201/meta, accessed on 13 December 2023)
C IV	$\longrightarrow$	C V	A. Müller, et al., J. Phys. B: At. Mol. Opt. Phys., **42**, 235602, 2009 [43] (https://iopscience.iop.org/article/10.1088/0953-4075/42/23/235602/meta, accessed on 13 December 2023)
C III	$\longrightarrow$	C IV	A. Müller, et al., Nucl. Instrum. Meth. B, **205**, 301, 2003 [44] (https://www.sciencedirect.com/science/article/pii/S0168583X02019699, accessed on 13 December 2023)
C III	$\longrightarrow$	C IV	S. W. J. Scully, et al., J. Phys. B: At. Mol. Opt. Phys., **38**, 1967, 2005 [45] (https://iopscience.iop.org/article/10.1088/0953-4075/38/12/011/meta, accessed on 13 December 2023)
C III	$\longrightarrow$	C IV	A. Müller, et al., J. Phys. B: At. Mol. Opt. Phys., **35**, L137, 2002 [46] (https://dx.doi.org/10.1088/0953-4075/35/7/101, accessed on 13 December 2023)
C III, N IV, O V	$\longrightarrow$	C IV, N V, O VI	A. Müller, et al., J. Phys. B: At. Mol. Opt. Phys., **43**, 225201, 2010 [28] (https://iopscience.iop.org/article/10.1088/0953-4075/43/22/225201/meta, accessed on 13 December 2023)
C II	$\longrightarrow$	C III	A. S. Schlachter, et al., J. Phys. B: At. Mol. Opt. Phys., **37**, L103, 2004 [47] (https://dx.doi.org/10.1088/0953-4075/37/5/L03, accessed on 13 December 2023)
O II	$\longrightarrow$	O III	A. M. Covington, et al., Phys. Rev. Lett. **87**, 243002, 2001 [29] (https://link.aps.org/doi/10.1103/PhysRevLett.87.243002, accessed on 13 December 2023)
O II	$\longrightarrow$	O III	A. Aguilar, et al., ApJS **146**, 467, 2003 [48] (https://dx.doi.org/10.1086/368077, accessed on 13 December 2023)
Ne IV, F III	$\longrightarrow$	Ne V, F IV	A. Aguilar, et al., J. Phys. B: At. Mol. Opt. Phys., **38**, 343, 2005 [49] (https://dx.doi.org/10.1088/0953-4075/38/4/003, accessed on 13 December 2023)
Ne III	$\longrightarrow$	Ne IV	S. N. Nahar, et al., Int. J. Mass Spectrom., **443**, 61–69, 2019 [50] (https://www.sciencedirect.com/science/article/pii/S1387380618304056, accessed on 13 December 2023)
Ne II	$\longrightarrow$	Ne III	A. M. Covington, et al., Phys. Rev. A **66**, 062710, 2002 [30] (https://link.aps.org/doi/10.1103/PhysRevA.66.062710, accessed on 13 December 2023)
Na$^-$	$\longrightarrow$	Na$^+$	A. M. Covington, et al., J. Phys. B: At. Mol. Opt. Phys., **34**, L735, 2001 [31] (https://dx.doi.org/10.1088/0953-4075/34/22/105, accessed on 13 December 2023)
Mg II, Al III	$\longrightarrow$	Mg III, Al IV	A. Aguilar, et al., Phys. Rev. A, **67**, 012701, 2003 [51] (https://journals.aps.org/pra/abstract/10.1103/PhysRevA.67.012701, accessed on 13 December 2023)

Table 1. *Cont.*

Photoionization			Reference
Al II	$\longrightarrow$	Al III	C. E. Hudson, et al., J. Phys. B: At. Mol. Opt. Phys., **38**, 2911, 2005 [52] (https://iopscience.iop.org/article/10.1088/0953-4075/38/16/005/meta, accessed on 13 December 2023)
CO^+	$\longrightarrow$	CO^{2+}	G. Hinojosa, et al., Phys. Rev. A, **66**, 032718, 2002 [53] (https://link.aps.org/doi/10.1103/PhysRevA.66.032718, accessed on 13 December 2023)
CO^+	$\longrightarrow$	O^+	G. Hinojosa, et al., J. Phys. B: At. Mol. Opt. Phys., **38**, 2701, 2005 [54] (https://dx.doi.org/10.1088/0953-4075/38/15/010, accessed on 13 December 2023)
P III, P IV	$\longrightarrow$	P IV, P V	L. Hernández, et al., J. Quant. Spectroc. Ra., **159**, 80–86, 2015 [55] (https://www.sciencedirect.com/science/article/pii/S0022407315000953, accessed on 13 December 2023)
P II	$\longrightarrow$	P III	S. N. Nahar, et al., J. Quant. Spectroc. Ra., **187**, 215–223, 2017 [56] (https://www.sciencedirect.com/science/article/pii/S002240731630365X?via%3Dihub, accessed on 13 December 2023)
Cl III	$\longrightarrow$	Cl IV	S. N. Nahar, et al., Atoms, **11**, 28, 2023 [57] (https://www.mdpi.com/2218-2004/11/2/28, accessed on 13 December 2023)
Cl II	$\longrightarrow$	Cl III	E. M. Hernández, et al., J. Quant. Spectroc. Ra., **151**, 217, 2015 [58] (https://www.sciencedirect.com/science/article/pii/S0022407314004191, accessed on 13 December 2023)
Ar VI	$\longrightarrow$	Ar VII	Jing Cheng Wang, et al., Phys. Rev. A, **75**, 062712, 2007 [59] (https://journals.aps.org/pra/abstract/10.1103/PhysRevA.75.062712, accessed on 13 December 2023)
Ar II	$\longrightarrow$	Ar III	A. M. Covington, et al., Phys. Rev. A **84**, 013413, 2011 [60] (https://journals.aps.org/pra/abstract/10.1103/PhysRevA.84.013413, accessed on 13 December 2023)
Ar II	$\longrightarrow$	Ar IV	A. Müller, et al., Phys. Rev. A, **103**, L031101, 2021 [61] (https://journals.aps.org/pra/abstract/10.1103/PhysRevA.103.L031101, accessed on 13 December 2023)
K III	$\longrightarrow$	K IV	G. A. Alna'Washi, et al., Phys. Rev. A, **90**, 023417, 2014 [62] (https://journals.aps.org/pra/abstract/10.1103/PhysRevA.90.023417, accessed on 13 December 2023)
Ca IV	$\longrightarrow$	Ca V	Ghassan A. Alna'washi, et al., Phys. Rev. A, **81**, 053416, 2010 [63] (https://journals.aps.org/pra/abstract/10.1103/PhysRevA.81.053416, accessed on 13 December 2023)
Ca II	$\longrightarrow$	Ca III	A. Müller, et al., J. Phys. B: At. Mol. Opt. Phys., **50**, 205001, 2017 [64] (https://iopscience.iop.org/article/10.1088/1361-6455/aa8ba8/pdf, accessed on 13 December 2023)
Sc III	$\longrightarrow$	Sc IV	S. Schippers, et al., Phys. Rev. Lett., **89**, 193002, 2002 [65] (https://link.aps.org/doi/10.1103/PhysRevLett.89.193002, accessed on 13 December 2023)
Sc III	$\longrightarrow$	Sc IV	S. Schippers, et al., Phys. Rev. A, **67**, 032702, 2003 [66] (https://link.aps.org/doi/10.1103/PhysRevA.67.032702, accessed on 13 December 2023)
Sc III	$\longrightarrow$	Sc IV	S. Schippers, et al., Nucl. Instrum. Meth. B, **205**, 297, 2003 [67] (https://www.sciencedirect.com/science/article/pii/S0168583X02019651, accessed on 13 December 2023)
Ti IV	$\longrightarrow$	Ti V	S. Schippers, et al., J. Phys. B: At. Mol. Opt. Phys., **37**, L209, 2004 [68] (https://dx.doi.org/10.1088/0953-4075/37/10/L02, accessed on 13 December 2023)
Fe IV, VI, VIII	$\longrightarrow$	Fe V, VII, IX	M. F. Gharaibeh, et al., Phys. Rev. A, **83**, 043412, 2011 [69] (https://journals.aps.org/pra/abstract/10.1103/PhysRevA.83.043412, accessed on 13 December 2023)
Zn II	$\longrightarrow$	Zn III	G. Hinojosa, et al., Mon. Not. R. Astron. Soc., **470**, 4048–4060, 2017 [70] (https://academic.oup.com/mnras/article/470/4/4048/3869632, accessed on 13 December 2023)
Se IV, Se VI	$\longrightarrow$	Se V, Se VII	D. A. Esteves, et al., J. Phys. B: At. Mol. Opt. Phys., **45**, 115201, 2012 [71] (https://iopscience.iop.org/article/10.1088/0953-4075/45/11/115201/meta, accessed on 13 December 2023)

Table 1. *Cont.*

Photoionization			Reference
Se III	⟶	Se IV	D. A. Macaluso, et al., Phys. Rev. A, **92**, 063424, 2015 [72] (https://journals.aps.org/pra/abstract/10.1103/PhysRevA.92.063424, accessed on 13 December 2023)
Se II	⟶	Se III	N. C. Sterling, et al., J. Phys. B: At. Mol. Opt. Phys., **44**, 025701, 2011 [73] (https://iopscience.iop.org/article/10.1088/0953-4075/44/2/025701/meta, accessed on 13 December 2023)
Se II	⟶	Se III	D. A. Esteves, et al., Phys. Rev. A, **84**, 013406, 2011 [23] (https://journals.aps.org/pra/abstract/10.1103/PhysRevA.84.013406, accessed on 13 December 2023)
Kr VI	⟶	Kr VII	M. Lu, et al., Phys. Rev. A. **74**, 012703, 2006 [27] (https://journals.aps.org/pra/abstract/10.1103/PhysRevA.74.012703, accessed on 13 December 2023)
Kr IV	⟶	Kr V	M. Lu, et al., Phys. Rev. A, **74**, 062701, 2006 [74] (https://link.aps.org/doi/10.1103/PhysRevA.74.062701, accessed on 13 December 2023)
Kr II	⟶	Kr III	G. Hinojosa, et al., Phys. Rev. A, **86**, 063402, 2012 [75] (https://journals.aps.org/pra/abstract/10.1103/PhysRevA.86.063402, accessed on 13 December 2023)
Xe V–VII	⟶	Xe VI–VIII	A. Aguilar, et al., Phys. Rev. A, **73**, 032717, 2006 [76] (https://journals.aps.org/pra/abstract/10.1103/PhysRevA.73.032717, accessed on 13 December 2023)
Xe IV	⟶	Xe V	E. D. Emmons, et al., Phys. Rev. A, **71**, 042704, 2005 [77] (https://link.aps.org/doi/10.1103/PhysRevA.71.042704, accessed on 13 December 2023)
Xe VIII	⟶	Xe IX	A Müller, et al., J. Phys. B: At. Mol. Opt. Phys., **47**, 215202, 2014 [78] (https://iopscience.iop.org/article/10.1088/0953-4075/47/21/215202, accessed on 13 December 2023)
W VI	⟶	W VII	A. Müller, et al., J. Phys. B: At. Mol. Opt. Phys., **52**, 195005, 2019 [79] (https://iopscience.iop.org/article/10.1088/1361-6455/ab39c8, accessed on 13 December 2023)
W V	⟶	W VI	A. Müller, et al., J. Phys. B: At. Mol. Opt. Phys., **50**, 085007, 2017 [80] (https://iopscience.iop.org/article/10.1088/1361-6455/aa65df, accessed on 13 December 2023)
W III–IV	⟶	W IV–V	B. M. McLaughlin, et al., J. Phys. B: At. Mol. Opt. Phys., **49**, 065201, 2016 [81] (https://iopscience.iop.org/article/10.1088/0953-4075/49/6/065201, accessed on 13 December 2023)
W II, IV, VI	⟶	W III, V, VII	A. Müller, et al., Phys. Scr., **T144**, 014052, 2011 [82] (https://iopscience.iop.org/article/10.1088/0031-8949/2011/T144/014052/meta, accessed on 13 December 2023)
W II	⟶	W III	A. Müller, et al., J. Phys. B: At. Mol. Opt. Phys., **48**, 235203, 2015 [22] (https://iopscience.iop.org/article/10.1088/0953-4075/48/23/235203, accessed on 13 December 2023)
Ce III–Ce V	⟶	Ce IV–Ce VI	A. Müller, et al., Phys. Rev. Lett., **101**, 133001, 2008 [83] (https://journals.aps.org/prl/abstract/10.1103/PhysRevLett.101.133001, accessed on 13 December 2023)
Ce II–Ce X	⟶	Ce III–Ce XI	M. Habibi, et al., Phys. Rev. A, **80**, 033407, 2009 [84] (https://journals.aps.org/pra/abstract/10.1103/PhysRevA.80.033407, accessed on 13 December 2023)

4. New Additions to NORAD-Atomic-Data

The database NORAD-Atomic-Data has been enhanced by additions of new data recently, as described below, of atomic processes.

(1). Among the data added, a significant amount of new data is related to spectral formation from photo-excitation cross-sections of atoms and ions. There are three types of such data: (i) Atomic data for X-ray spectroscopy, especially for K-α and K-β transitions needed for the resonance fluorescence effect predicted by Pradhan et al. [85] for biomedical applications. This effect was later observed [86] and was interpreted [87] as shown in

Figure 2; (ii) Photoexcitation data for spectral formation by ions of bio-signature elements, such as phosphorus, e.g., [88]. (iii) Atomic data for spectroscopy of lanthanides of neutral-to-low ionization stages that may relate to the electromagnetic waves created during a kilonovae event of a merger of two neutron stars or black holes, e.g., [89].
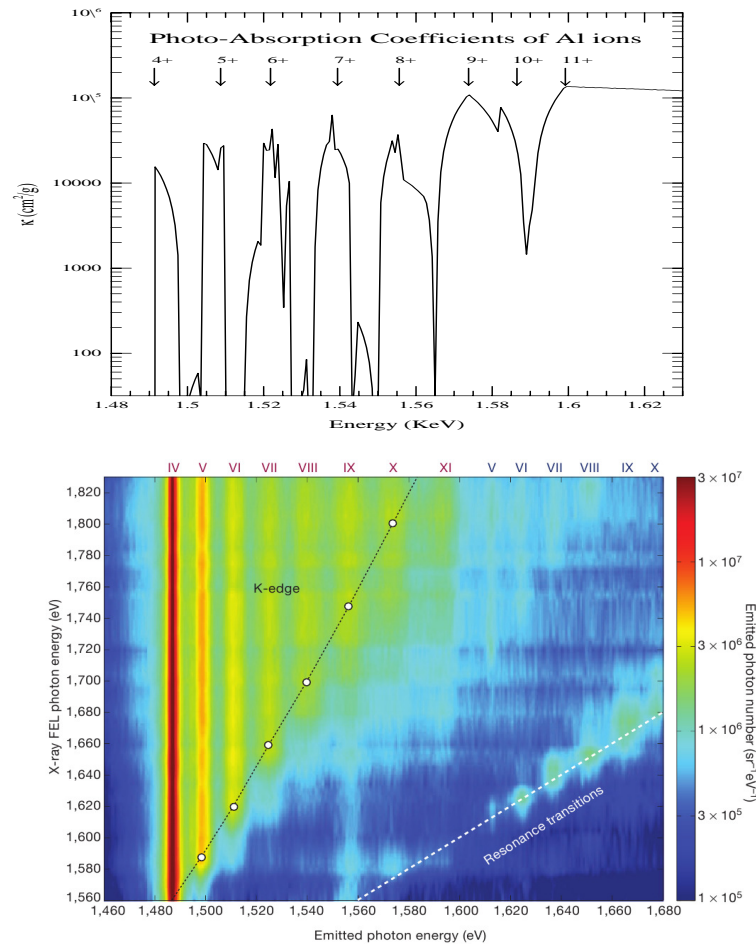
Figure 2. K_α resonance fluorescence in Al plasma [87]. Top: Theoretically computed K_α absorption features in Al ions isoelectronic with F to He are shown (eight ionization states are labeled in the top panel and Roman numerals in the bottom panel) in the energy range of 1.48–1.62 keV. All contributing K_α transition strengths are added together and shown in terms of X-ray attenuation coefficients (cm^2/g) (convoluted over a Gaussian FWHM of 10 eV). Bottom: Experimental measurements from the LCLS-XFEL [86] (reproduced with permission). The white dashed line on the right shows the six resonant transitions with increasing K_α emission intensity corresponding to the theoretical absorption complexes. The observed K_α features appear when the XFEL energy equals the emitted photon energy. Although there is a shift in energy between the prediction and observation, the resonant fluorescent features are clearly seen.

(2). The second addition is the inclusion of collisional data for collision strengths and rate coefficients for electron-impact excitation (EIE). NORAD-Atomic-Data considered almost no collisional data in the past since these data for various atomic systems are available from TIPbase [7] and from other investigators. However, for possible plasma diagnostics, NORAD-Atomic-Data has started to include these collisional data, e.g., for Ca IV [90].

(3). The third addition is experimental data for energy levels, and oscillator strengths included in the database. The NIST database [15] is the main source for compiled and evaluated experimental oscillator strengths and radiative decay rates. We have added large sets of experimental energy levels and transition parameters of a number of heavy ions,

obtained mainly from the leading spectroscopy laboratory of Aligarh Muslim University in India. These files contain complete sets of transitions that were measured in comparison to the evaluated sets available at the NIST. The added data are currently for eight ions, Ag III [91], Ag-IV [92], Au V [93], Bi IV [94], Hg III [95], Hg-IV [96], Hg V [93], and Hg-VI [93].

For the transition parameters, they used a vacuum spectrograph for the measurement of spectral lines from exposures created by the discharge of electrodes, containing the sample, with a trigger module of high-voltage electrical pulse. Details of their experiments, calibration, and analysis are given in their papers as referred with the ions above.

Aligarh lab has produced spectral data for many ions. However, currently available data are largely in pdf-formatted files, which were saved with their publications. More data will be added to NORAD-Atomic-Data when the authors provide the data files converted to ASCII format that can be read by programs.

(4). The fourth addition is the inclusion of experimental data for photoionization cross-sections. Most experimental set-ups are typically synchrotron-based, such as the Advanced Light Source (ALS) of synchrotron at Lawrence Berkeley National Lab (LBNL), set-ups at the University of Paris-SUD, Aahus University, and BESSY and PETRA in Germany. The other set-up that has been in use is laser-induced excited state photoionization in a few labs in Pakistan and in University of Nebraska. Among the experimental photoionization cross-section data available at NORAD-Atomic-Data are for ions such as Cl III, Cl II, K II, etc.

(5). The fifth addition to NORAD-Atomic-Data is a web-based interactive feature to obtain line ratios for plasma diagnostics. NORAD-Atomic-Data has all the basic radiative data, except for the collisional data for EIE, to calculate the line ratio diagnostics for many atoms and ions. Our recent study on line ratios of P II by [97], with the inclusion of the electron–ion recombination cascade effect that was known to have an impact but not considered in the astrophysical models before, demonstrated that the effect can lower or increase the line ratios. Figure 3 presents an exemplary impact of electron–ion recombination on line ratios (red) curve compared to that without the effect (dark red) on the low-lying transitions in P II [97].
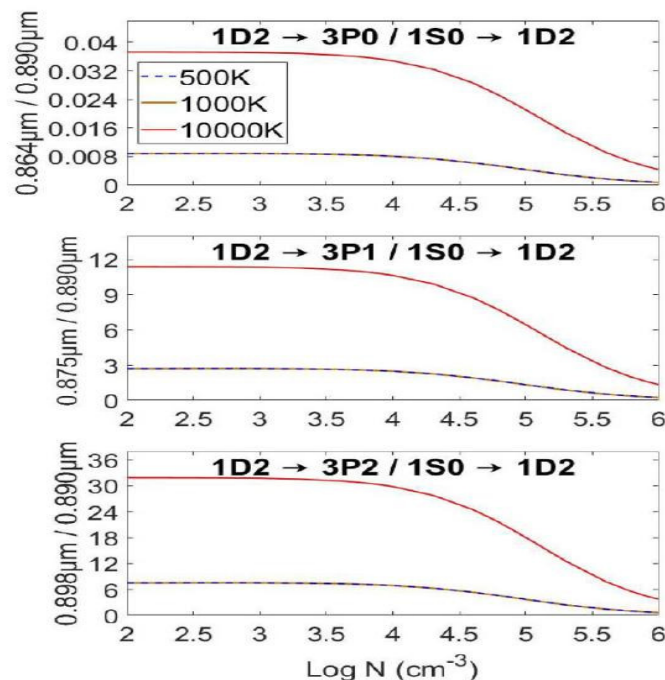
Figure 3. Emissivity ratios of [P II] lines at ionospheric and nebular temperatures 500 K, 1000 K, and 10,000 K lying within and potentially observed by JWST spectrometers. While 500 K and 1000 K lines (dark red) appear to be identical, they differ by a few percentage points, far less than the difference from the 10,000 K line [97].

We have computed the relevant atomic quantities in large sets that can be used to compute the line ratios for diagnostics over a large range of temperatures and densities. A preliminary version of the code is in operation at the web-based interactive feature for computing the line ratios at any temperature and density.

5. Conclusions

An overview with general outlines of contents on the new additions to the database NORAD-Atomic-Data is presented. There are six additions that have been discussed for the expansion of the database. Significant enhancements of data are due to additions of experimental data, not included before, and data for photo-absorption spectral features.

Testing of data for accuracy is given a high priority. The majority of data have been obtained from the ab initio R-matrix method. Results using atomic structure calculations have also been added for cases where they provide good accuracy, such as for X-ray or high-energy regions. In these regions perturbations and electron–electron interactions are relatively negligible. Data from atomic structure calculations has also been included for cases for which large amount of data are needed, such as for large atomic systems of lanthanides, and for which R-matrix calculations are prohibitive due to large numerical size.

While a theoretical overview along with description of data, accuracy, and benchmarking of the online database were presented in the earlier paper on the database [1], here we present a general overview of the experimental background, particularly of photoionization.

Future directions include the following:

(i) Include more data, both radiative and collisional, with publications;

(ii) Include computer programs that can read the data files and process the data to calculate the quantities of interest;

(iii) Add more data for the web-based feature to compute spectral line ratios of other atoms and ions for astrophysical applications;

(iv) Create an option for the selection of partial data, such as for a particular wavelength range.

Author Contributions: Conceptualization, S.N.N. and G.H.-A.; Methodology, S.N.N. and G.H.-A.; Software, S.N.N. and G.H.-A.; Validation, S.N.N. and G.H.-A.; Formal analysis, S.N.N. and G.H.-A.; Investigation, S.N.N. and G.H.-A.; Resources, S.N.N. and G.H.-A.; Data curation, S.N.N. and G.H.-A.; Writing—original draft, S.N.N. and G.H.-A.; Writing—review & editing, S.N.N. and G.H.-A.; Visualization, S.N.N. and G.H.-A.; Supervision, S.N.N.; Project administration, S.N.N.; Funding acquisition, S.N.N. All authors have read and agreed to the published version of the manuscript.

Data Availability Statement: All data are available at database NORAD-Atomic-Data https://norad.astronomy.osu.edu/, accessed on 13 December 2023.

Conflicts of Interest: The authors declare no conflicts of interest.

Acronyms

List of acronyms used in this article.

NORAD	Nahar OSU RADiative
LBNL	Lawrence Berkeley National Laboratory
ALS	Advanced Light Source
OP	Opacity Project
IP	Iron Project
SNN	Sultana N. Nahar
TOPbase	The Opacity Project Atomic Database
TIPbase	The Iron Project Atomic Database

SS	SUPERSTRUCTURE
BPRM	Relativistic Breit–Pauli R-matrix
NIST	National Institute of Standards and Technology
CC	Close Coupling Approximation
DR	Intermediate Recombination
AI	Autoionization
DES	Dielectronic Recombination
EIE	Electron-Impact Excitation
MBT	Merged Beam Technique
FWHM	Full Width Half Maximum
ECR	Electron Cyclotron Resonance
LCLS-XFEL	Linac Coherent-Light Source X-ray free-electron laser
JWST	James Webb Space Telescope
BESSY	Berlin Electron Storage Ring Society for Synchrotron Radiation (From German name)
PETRA	Positron-Electron Tandem Ring Accelerator

References

1. Nahar, S. Database NORAD-Atomic-Data for atomic processes in plasma. *Atoms* **2020**, *8*, 68. [CrossRef]
2. Nahar, S.N. NaharOSURadiative(NORAD)-Atomic-Data. The Ohio State University. 2007. Available online: http://norad.astronomy.osu.edu/ (accessed on 7 August 2007).
3. Seaton, M.J. Atomic data for opacity calculations. I. General description. *J. Phys. B* **1987**, *20*, 6363–6378. [CrossRef]
4. *The Opacity Project*; The Opacity Project Team, Institute of Physics Publishing: London, UK, 1995; Volume 1.
5. Hummer, D.G.; Berrington, K.A.; Eissner, W.; Pradhan, A.K.; Saraph, H.E.; Tully, J.A. Atomic data from the IRON Project. 1: Goals and methods. *Astron. Astrophys.* **1993**, *279*, 298–309.
6. Cunto, W.; Mendoza, C.; Ochsenbein, F.; Zeippen, C.J. TOPbase at the CDS. *Astron. Astrophys.* **1993**, *275*, L5–L8. Available online: http://cdsweb.u-strasbg.fr/topbase/topbase.html (accessed on 27 September 1993).
7. TIPbase. 2001. Available online: http://cdsweb.u-strasbg.fr/tipbase/home.html (accessed on 27 September 2020).
8. Pradhan, A.K.; Nahar, S.N. *Atomic Astrophysics and Spectroscopy*; Cambridge University Press: Cambridge, UK, 2011.
9. Berrington, K.A.; Burke, P.G.; Butler, K.; Seaton, M.J.; Storey, P.J.; Taylor, K.T.; Yan, Y. Atomic data for opacity calculations. II. Computational methods. *J. Phys. B* **1987**, *20*, 6379–6397. [CrossRef]
10. Berrington, K.A.; Eissner, W.; Norrington, P.H. RMATRIX1: Belfast atomic R-matrix codes. *Comput. Phys. Commun.* **1995**, *92*, 290–420. [CrossRef]
11. Nahar, S.N. Atomic Data from the Iron Project VII. Radiative dipole transition probabilities for Fe II. *Astron. Astrophys.* **1995**, *293*, 967–977.
12. Nahar, S.N. Fine structure transitions in Fe XIV. *New Astron.* **2013**, *21*, 8–16. [CrossRef]
13. Eissner, W.; Jones, M.; Nussbaumer, H. Techniques for the calculation of atomic structures and radiative data including relativistic corrections. *Comput. Phys. Commun.* **1974**, *8*, 270–306. [CrossRef]
14. Nahar, S.N.; Eissner, W.; Chen, G.X.; Pradhan, A.K. Atomic data from the Iron Project-LIII. Relativistic allowed and forbidden transitionstic probabilities for Fe XVII. *Astron. Astrophys.* **2003**, *408*, 789–8016. [CrossRef]
15. NIST. Available online: https://physics.nist.gov/PhysRefData/ASD/levels_form.html (accessed on 1 January 1996).
16. Nahar, S.N.; Pradhan, A.K. Unified Treatment of Electron-Ion Recombination in the Close Coupling Approximation. *Phys. Rev. A* **1994**, *49*, 1816. [CrossRef] [PubMed]
17. Zhang, H.L.; Nahar, S.N.; Pradhan, A.K. Close coupling R-matrix calculations for electron-ion recombination cross sections. *J. Phys. B* **1999**, *32*, 1459–1479. [CrossRef]
18. Nahar, S.N.; Pradhan, A.K. Electron-ion recombination in the close coupling approximation. *Phys. Rev. Lett.* **1992**, *68*, 1488–1491. [CrossRef] [PubMed]
19. Bell, R.H.; Seaton, M.J. Dielectronic recombination: I. General theory. *J. Phys. B* **1985**, *18*, 1589–1629. [CrossRef]
20. Phaneuf, R.A.; Havener, C.C.; Dunn, G.H.; Müller, A. Merged-beams experiments in atomic and molecular physics. *Rep. Prog. Phys.* **1999**, *62*, 1143. [CrossRef]
21. Margaritondo, G. Synchrotron light: A success story over six decades. *Riv. Nuovo Cimento* **2017**, *40*, 411–471. [CrossRef]
22. Müller, A.; Schippers, S.; Hellhund, J.; Holste, K.; Kilcoyne, A.L.D.; Phaneuf, R.A.; Ballance, C.P.; McLaughlin, B.M. Single-photon single ionization of W+ ions: Experiment and theory. *J. Phys. B At. Mol. Opt. Phys.* **2015**, *48*, 235203. [CrossRef]
23. Esteves, D.A.; Bilodeau, R.C.; Sterling, N.C.; Phaneuf, R.A.; Kilcoyne, A.L.D.; Red, E.C.; Aguilar, A. Absolute high-resolution Se+ photoionization cross-section measurements with Rydberg-series analysis. *Phys. Rev. A* **2011**, *84*, 013406. [CrossRef]
24. Domke, M.; Schulz, K.; Remmers, G.; Kaindl, G.; Wintgen, D. High-resolution study of 1 P0 double-excitation states in helium. *Phys. Rev. A* **1996**, *53*, 1424–1438. [CrossRef]
25. King, G.C.; Tronc, M.; Read, F.H.; Bradford, R.C. An investigation of the structure near the L2,3 edges of argon, the M4,5 edges of kryton and the N4,5 edges of xenon, using electron impact with high resolution. *J. Phys. B At. Mol. Opt.* **1977**, *10*, 2479–2495. [CrossRef]

26. Kramida, A.; Ralchenko, Y.; Reader, J.; NIST ASD Team. *NIST Atomic Spectra Database*; Version 5.10, Online; National Institute of Standards and Technology: Gaithersburg, MD, USA, 2022. [CrossRef]

27. Lu, M.; Gharaibeh, M.F.; Alna'washi, G.; Phaneuf, R.A.; Kilcoyne, A.L.D.; Levenson, E.; Schlachter, A.S.; Müller, A.; Schippers, S.; Jacobi, J.; et al. Photoionization and electron-impact ionization of Kr5+. *Phys. Rev. A* **2006**, *74*, 012703. [CrossRef]

28. Müller, A.; Schippers, S.; Phaneuf, R.A.; Kilcoyne, A.L.D.; Bräuning, H.; Schlachter, A.S.; Lu, M.; McLaughlin, B.M. State-resolved valence shell photoionization of Be-like ions: Experiment and theory. *J. Phys. B At. Mol. Opt. Phys.* **2010**, *43*, 225201. [CrossRef]

29. Covington, A.M.; Aguilar, A.; Covington, I.R.; Gharaibeh, M.; Shirley, C.A.; Phaneuf, R.A.; Alvarez, I.; Cisneros, C.; Hinojosa, G.; Bozek, J.D.; et al. Photoionization of Metastable O+ Ions: Experiment and Theory. *Phys. Rev. Lett.* **2001**, *87*, 243002. [CrossRef] [PubMed]

30. Covington, A.M.; Aguilar, A.; Covington, I.R.; Gharaibeh, M.F.; Hinojosa, G.; Shirley, C.A.; Phaneuf, R.A.; Álvarez, I.; Cisneros, C.; Dominguez-Lopez, I.; et al. Photoionization of Ne+ using synchrotron radiation. *Phys. Rev. A* **2002**, *66*, 062710. [CrossRef]

31. Covington, A.M.; Aguilar, A.; Davis, V.T.; Alvarez, I.; Bryant, H.C.; Cisneros, C.; Halka, M.; Hanstorp, D.; Hinojosa, G.; Schlachter, A.S.; et al. Correlated processes in inner-shell photodetachment of the Na-ion. *J. Phys. B At. Mol. Opt. Phys.* **2001**, *34*, L735. [CrossRef]

32. Scully, S.W.J.; Alvarez, I.; Cisneros, C.; Emmons, E.D.; Gharaibeh, M.F.; Leitner, D.; Lubell, M.S.; Müller, A.; Phaneuf, R.A.; Püttner, R.; et al. Doubly excited resonances in the photoionization spectrum of Li +: Experiment and theory. *J. Phys. B At. Mol. Opt. Phys.* **2006**, *39*, 3957. [CrossRef]

33. Schmidt, V. Photoionization of atoms using synchrotron radiation. *Rep. Prog. Phys.* **1992**, *55*, 1483. [CrossRef]

34. Sonntag, B.; Zimmermann, P. XUV spectroscopy of metal atoms. *Rep. Prog. Phys.* **1992**, *55*, 911. [CrossRef]

35. West, J.B. Photoionization of atomic ions. *J. Phys. B At. Mol. Opt.* **2001**, *34*, R45. [CrossRef]

36. Lyon, I.C.; Peart, B.; West, J.B.; Dolder, K. Measurements of absolute cross sections for the photoionisation of Ba+ ions. *J. Phys. B At. Mol. Opt.* **1986**, *19*, 4137. [CrossRef]

37. Kjeldsen, H. Photoionization cross sections of atomic ions from merged-beam experiments. *J. Phys. B At. Mol. Opt.* **2006**, *39*, R325. [CrossRef]

38. Martins, M.; Godehusen, K.; Richter, T.; Wernet, P.; Zimmermann, P. Open shells and multi-electron interactions: Core level photoionization of the 3d metal atoms. *J. Phys. B At. Mol. Opt.* **2006**, *39*, R79. [CrossRef]

39. Schippers, S.; Müller, A. Photoionization of Astrophysically Relevant Atomic Ions at PIPE. *Atoms* **2020**, *8*, 45. [CrossRef]

40. Müller, A.; Schippers, S.; Phaneuf, R.A.; Scully, S.W.J.; Aguilar, A.; Cisneros, C.; Gharaibeh, M.F.; Schlachter, A.S.; McLaughlin, B.M. K-shell photoionization of ground-state Li-like boron ions [B^{2+}]: Experiment and theory. *J. Phys. B At. Mol. Opt. Phys.* **2010**, *43*, 135602. [CrossRef]

41. Schippers, S.; Müller, A.; McLaughlin, B.M.; Aguilar, A.; Cisneros, C.; Emmons, E.D.; Gharaibeh, M.F.; Phaneuf, R.A. Photoionization studies of the B^+ valence shell: Experiment and theory. *J. Phys. B At. Mol. Opt. Phys.* **2003**, *36*, 3371. [CrossRef]

42. Müller, A.; Schippers, S.; Phaneuf, R.A.; Scully, S.W.J.; Aguilar, A.; Cisneros, C.; Gharaibeh, M.F.; Schlachter, A.S.; McLaughlin, B.M. K-shell photoionization of Be-like boron (B^+) ions: Experiment and theory. *J. Phys. B At. Mol. Opt. Phys.* **2014**, *47*, 135201. [CrossRef]

43. Müller, A.; Schippers, S.; Phaneuf, R.A.; Scully, S.W.J.; Aguilar, A.; Covington, A.M.; Álvarez, I.; Cisneros, C.; Emmons, E.D.; Gharaibeh, M.F.; et al. K-shell photoionization of ground-state Li-like carbon ions [C^{3+}]: Experiment, theory and comparison with time-reversed photorecombination. *J. Phys. B At. Mol. Opt. Phys.* **2009**, *42*, 235602. [CrossRef]

44. Müller, A.; Phaneuf, R.A.; Aguilar, A.; Gharaibeh, M.F.; Schlachter, A.S.; Álvarez, I.; Cisneros, C.; Hinojosa, G.; McLaughlin, B.M. Photoionization of C^{2+} ions. *Nucl. Instruments Methods Phys. Res. Sect. Beam Interact. Mater. Atoms.* **2003**, *205*, 301–305. [CrossRef]

45. Scully, S.W.J.; Aguilar, A.; Emmons, E.D.; Phaneuf, R.A.; Halka, M.; Leitner, D.; Levin, J.C.; Lubell, M.S.; Püttner, R.; Schlachter, A.S.; et al. K-shell photoionization of Be-like carbon ions: Experiment and theory for C^{2+}. *J. Phys. B At. Mol. Opt. Phys.* **2005**, *38*, 1967. [CrossRef]

46. Müller, A.; Phaneuf, R.A.; Aguilar, A.; Gharaibeh, M.F.; Schlachter, A.S.; Alvarez, I.; Cisneros, C.; Hinojosa, G.; McLaughlin, B.M. Photoionization of C^{2+} ions: Time-reversed recombination of C^{3+} with electrons. *J. Phys. B At. Mol. Opt. Phys.* **2002**, *35*, L137. [CrossRef]

47. Schlachter, A.S.; Sant'Anna, M.M.; Covington, A.M.; Aguilar, A.; Gharaibeh, M.F.; Emmons, E.D.; Scully, S.W.J.; Phaneuf, R.A.; Hinojosa, G.; Álvarez, I.; et al. Lifetime of a K-shell vacancy in atomic carbon created by $1s \rightarrow 2p$ photoexcitation of C^+. *J. Phys. B At. Mol. Opt. Phys.* **2004**, *37*, L103. [CrossRef]

48. Aguilar, A.; Covington, A.M.; Hinojosa, G.; Phaneuf, R.A.; Álvarez, I.; Cisneros, C.; Bozek, J.D.; Dominguez, I.; Sant'Anna, M.M.; Schlachter, A.S.; et al. Absolute Photoionization Cross Section Measurements of O II Ions from 29.7 to 46.2 eV. *ApJS* **2003**, *146*, 467. [CrossRef]

49. Aguilar, A.; Emmons, E.D.; Gharaibeh, M.F.; Covington, A.M.; Bozek, J.D.; Ackerman, G.; Canton, S.; Rude, B.; Schlachter, A.S.; Hinojosa, G.; et al. Photoionization of ions of the nitrogen isoelectronic sequence: Experiment and theory for F^{2+} and $^{3+}$. *J. Phys. B At. Mol. Opt. Phys.* **2005**, *38*, 343. [CrossRef]

50. Nahar, S.N.; Covington, A.M.; Kilcoyne, D.; Davis, V.T.; Thompson, J.F.; Hernández, E.M.; Antillón, A.; Juárez, A.M.; Morales-Mori, A.; Hinojosa, G. Single-photon photoionization of oxygen-like Ne III. *Int. J. Mass Spectrom.* **2019**, *443*, 61–69. [CrossRef]

51. Aguilar, A.; West, J.B.; Phaneuf, R.A.; Brooks, R.L.; Folkmann, F.; Kjeldsen, H.; Bozek, J.D.; Schlachter, A.S.; Cisneros, C. Photoionization of isoelectronic ions: Mg^+ and Al^{2+}. *Phys. Rev. A* **2003**, *67*, 012701.

52. Hudson, C.E.; West, J.B.; Bell, K.L.; Aguilar, A.; Phaneuf, R.A.; Folkmann, F.; Kjeldsen, H.; Bozek, J.; Schlachter, A.S.; Cisneros, C. A theoretical and experimental study of the photoionization of AlII. *J. Phys. B At. Mol. Opt. Phys.* **2005**, *38*, 2911.

53. Hinojosa, G.; Covington, A.M.; Phaneuf, R.A.; Sant'Anna, M.M.; Hernez, R.; Covington, I.R.; Domínguez, I.; Bozek, J.D.; Schlachter, A.S.; Álvarez, I.; et al. Formation of long-lived CO2+ via photoionization of CO^+. *Phys. Rev. A* **2002**, *66*, 032718. [CrossRef]

54. Hinojosa, G.; Sant'Anna, M.M.; Covington, A.M.; Phaneuf, R.A.; Covington, I.R.; Domínguez, I.; Schlachter, A.S.; Alvarez, I.; Cisneros, C. Photofragmentation of ionic carbon monoxide. *J. Phys. B At. Mol. Opt. Phys.* **2005**, *38*, 2701. [CrossRef]

55. Hernández, L.; Covington, A.M.; Hernández, E.M.; Antillón, A.; Morales-Mori, A.; Chartkunch, K.; Aguilar, A.; Hinojosa, G. Single photoionization of aluminum-like P^{2+} and magnesium-like P^{3+}. *J. Quant. Spectrosc. Radiat. Transf.* **2015**, *159*, 80–86. [CrossRef]

56. Nahar, S.N.; Hernández, E.M.; Hernández, L.; Antillon, A.; Morales-Mori, A.; González, O.; Covington, A.M.; Chartkunch, K.C.; Hanstorp, D.; Juárez, A.M.; et al. Photoionization of P^+: Experiment and theory. *J. Quant. Spectrosc. Radiat. Transf.* **2017**, *187*, 215–223. [CrossRef]

57. Nahar, S.N.; Hernández, E.M.; Kilcoyne, D.; Antillón, A.; Covington, A.M.; González-Magaña, O.; Hernández, L.; Davis, V.; Calabrese, D.; Morales-Mori, A.; et al. Experimental and Theoretical Study of Photoionization of Cl III. *Atoms* **2023**, *11*, 28. [CrossRef]

58. Hernández, E.M.; Juárez, A.M.; Kilcoyne, A.L.D.; Aguilar, A.; Hernández, L.; Antillón, A.; Macaluso, D.; Morales-Mori, A.; González-Magaña, O.; Hanstorp, D.; et al. Absolute measurements of chlorine Cl+ cation single photoionization cross section. *J. Quant. Spectrosc. Radiat. Transf.* **2015**, *151*, 217–223. [CrossRef]

59. Wang, J.C.; Lu, M.; Esteves, D.; Habibi, M.; Alna'washi, G.; Phaneuf, R.A.; Kilcoyne, A.L.D. Photoionization and electron-impact ionization of Ar^{5+}. *Phys. Rev. A* **2007,** *75*, 062712.

60. Covington, A.M.; Aguilar, A.; Covington, I.R.; Hinojosa, G.; Shirley, C.A.; Phaneuf, R.A.; Álvarez, I.; Cisneros, C.; Dominguez-Lopez, I.; Sant'Anna, M.M.; et al. Valence-shell photoionization of chlorinelike Ar^+ ions. *Phys. Rev. A* **2011**, *84*, 013413. [CrossRef]

61. Müller, A.; Kilcoyne, A.L.D.; Phaneuf, R.A.; Holste, K.; Schippers, S.; Kheifets, A.S. Direct double ionization of the Ar^+ M shell by a single photon. *Phys. Rev. A* **2021**, *103*, L031101. [CrossRef]

62. Alna'Washi, G.A.; Lu, M.; Habibi, M.; Esteves-Macaluso, D.; Wang, J.C.; Phaneuf, R.A.; Kilcoyne, A.L.D.; Cisneros, C.; McLaughlin, B.M. Valence-shell single photoionization of chlorine-like K^{2+} ions: Experiment and theory. *Phys. Rev. A* **2014**, *90*, 023417. [CrossRef]

63. Alna'washi, G.A.; Lu, M.; Habibi, M.; Phaneuf, R.A.; Kilcoyne, A.L.D.; Schlachter, A.S.; Cisneros, C.; McLaughlin, B.M. Valence-shell photoionization of the chlorinelike Ca^{3+} ion. *Phys. Rev. A* **2010**, *81*, 053416. [CrossRef]

64. Müller, A.; Schippers, S.; Phaneuf, R.A.; Covington, A.M.; Aguilar, A.; Hinojosa, G.; Bozek, J.; Sant'Anna, M.M.; Schlachter, A.S.; Cisneros, C.; et al. Photoionisation of Ca+ ions in the valence-energy region 20–56 eV: Experiment and theory. *J. Phys. B At. Mol. Opt. Phys.* **2017**, *50*, 205001. [CrossRef]

65. Schippers, S.; Müller, A.; Ricz, S.; Bannister, M.E.; Dunn, G.H.; Bozek, J.; Schlachter, A.S.; Hinojosa, G.; Cisneros, C.; Aguilar, A.; et al. Experimental Link of Photoionization of Sc^{2+} to Photorecombination of Sc^{3+}: An Application of Detailed Balance in a Unique Atomic System. *Phys. Rev. Lett.* **2002**, *89*, 193002. [CrossRef] [PubMed]

66. Schippers, S.; Müller, A.; Ricz, S.; Bannister, M.E.; Dunn, G.H.; Schlachter, A.S.; Hinojosa, G.; Cisneros, C.; Aguilar, A.; Covington, A.M.; et al. Photoionization of Sc^{2+} Ions by Synchrotron Radiation: Measurements and Absolute Cross Sections in the Photon Energy Range 23–68 eV. *Phys. Rev. A* **2003**, *67*, 032702. [CrossRef]

67. Schippers, S.; Müller, A.; Ricz, S.; Bannister, M.E.; Dunn, G.H.; Bozek, J.; Schlachter, A.S.; Hinojosa, G.; Cisneros, C.; Aguilar, A.; et al. Photoionization of Sc^{2+}: Experimental Link with Photorecombination of Sc3+ by Application of Detailed Balance. *Nucl. Instrum. Methods B* **2003**, *205*, 297–300. [CrossRef]

68. Schippers, S.; Müller, A.; Phaneuf, R.A.; van Zoest, T.; Álvarez, I.; Cisneros, C.; Emmons, E.D.; Gharaibeh, M.F.; Hinojosa, G.; Schlachter, A.S.; et al. Threshold truncation of a 'giant' dipole resonance in photoionization of Ti^{3+}. *J. Phys. B At. Mol. Opt. Phys.* **2004**, *37*, L209–L216. [CrossRef]

69. Gharaibeh, M.F.; Aguilar, A.; Covington, A.M.; Emmons, E.D.; Scully, S.W.J.; Phaneuf, R.A.; Müller, A.; Bozek, J.D.; Kilcoyne, A.L.D.; Schlachter, A.S.; et al. Photoionization measurements for the iron isonuclear sequence Fe^{3+}, Fe^{5+}, and Fe^{7+}. *Phys. Rev. A* **2011**, *83*, 043412. [CrossRef]

70. Hinojosa, G.; Davis, V.T.; Covington, A.M.; Thompson, J.S.; Kilcoyne, A.L.D.; Antillón, A.; Hernández, E.M.; Calabrese, D.; Morales-Mori, A.; Juárez, A.M.; et al. Single photoionization of the Zn ii ion in the photon energy range 17.5–90.0 eV: Experiment and theory. *Mon. Not. R. Astron. Soc.* **2017**, *470*, 4048–4060. [CrossRef]

71. Esteves, D.A.; Aguilar, A.; Bilodeau, R.C.; Phaneuf, R.A.; Kilcoyne, A.L.D.; Red, E.C.; Sterling, N.C. Absolute single photoionization cross-section measurements of Se^{3+} and Se^{5+}. *J. Phys. B At. Mol. Opt. Phys.* **2012**, *45*, 115201. [CrossRef]

72. Macaluso, D.A.; Aguilar, A.; Kilcoyne, A.L.D.; Red, E.C.; Bilodeau, R.C.; Phaneuf, R.A.; Sterling, N.C.; McLaughlin, B.M. Absolute single-photoionization cross sections of Se^{2+}: Experiment and theory. *Phys. Rev. A* **2015**, *92*, 063424. [CrossRef]

73. Sterling, N.C.; Esteves, D.A.; Bilodeau, R.C.; Kilcoyne, A.L.D.; Red, E.C.; Phaneuf, R.A.; Aguilar, A. Experimental photoionization cross-section measurements in the ground and metastable state threshold region of Se^+. *J. Phys. B At. Mol. Opt. Phys.* **2011**, *44*, 025701. [CrossRef]

74. Lu, M.; Gharaibeh, M.F.; Alna'washi, G.; Phaneuf, R.A.; Kilcoyne, A.L.D.; Levenson, E.; Schlachter, A.S.; Cisneros, C.; Hinojosa, G. Photoionization and electron-impact ionization of Kr^{3+}. *Phys. Rev. A* **2006**, *74*, 012701.

75. Hinojosa, G.; Covington, A.M.; Alna-Washi, G.A.; Lu, M.; Phaneuf, R.A.; Sant-Anna, M.M.; Cisneros, C.; Alvarez, I.; Aguilar, A.; Kilcoyne, A.L.D.; et al. Valence-shell single photoionization of Kr+ ions: Experiment and theory. *Phys. Rev. A* **2012**, *86*, 063402. [CrossRef]

76. Aguilar, A.; Gillaspy, J.D.; Gribakin, G.F.; Phaneuf, R.A.; Gharaibeh, M.F.; Kozlov, M.G.; Bozek, J.D.; Kilcoyne, A.L.D. Absolute photoionization cross sections for Xe^{4+}, Xe^{5+}, and Xe^{6+} near 13.5 nm: Experiment and theory. *Phys. Rev. A* **2006**, *73*, 032717. [CrossRef]

77. Emmons, E.D.; Aguilar, A.; Gharaibeh, M.F.; Scully, S.W.J.; Phaneuf, R.A.; Kilcoyne, A.L.D.; Schlachter, A.S.; Álvarez, I.; Cisneros, C.; Hinojosa, G. Photoionization and electron-impact ionization of Xe^{3+}. *Phys. Rev. A* **2005**, *71*, 042704. [CrossRef]

78. Müller, A.; Schippers, S.; Esteves-Macaluso, D.; Habibi, M.; Aguilar, A.; Kilcoyne, A.L.D.; Phaneuf, R.A.; Ballance, C.P.; McLaughlin, B.M. Valence-shell photoionization of Ag-like Xe^{7+} ions: Experiment and theory. *J. Phys. B At. Mol. Opt. Phys.* **2014**, *47*, 215202. [CrossRef]

79. Müller, A.; Schippers, S.; Hellhund, J.; Kilcoyne, A.L.D.; Phaneuf, R.A.; McLaughlin, B.M. Photoionization of tungsten ions: experiment and theory for W^{5+}. *J. Phys. B At. Mol. Opt. Phys.* **2019**, *52*, 195005. [CrossRef]

80. Müller, A.; Schippers, S.; Hellhund, J.; Kilcoyne, A.L.D.; Phaneuf, R.A.; McLaughlin, B.M. Photoionization of tungsten ions: experiment and theory for W^{4+}. *J. Phys. B At. Mol. Opt. Phys.* **2017**, *50*, 085007. [CrossRef]

81. McLaughlin, B.M.; Ballance, C.P.; Schippers, S.; Hellhund, J.; Kilcoyne, A.L.D.; Phaneuf, R.A.; Müller, A. Photoionization of tungsten ions: Experiment and theory for w^{2+} and w^{3+}. *J. Phys. B At. Mol. Opt. Phys.* **2016**, *49*, 065201. [CrossRef]

82. Müller, A.; Schippers, S.; Kilcoyne, A.L.D.; Esteves, D. Photoionization of tungsten ions with synchrotron radiation. *Phys. Scr.* **2011**, *2011*, 014052. [CrossRef]

83. Müller, A.; Schippers, S.; Habibi, M.; Esteves, D.; Wang, J.C.; Phaneuf, R.A.; Kilcoyne, A.L.D.; Aguilar, A.; Dunsch, L. Significant redistribution of Ce 4d oscillator strength observed in photoionization of endohedral Ce@C+82 ions. *Phys. Rev. Lett.* **2008**, *101*, 133001. [CrossRef] [PubMed]

84. Habibi, M.; Esteves, D.A.; Phaneuf, R.A.; Kilcoyne, A.L.D.; Aguilar, A.; Cisneros, C. Photoionization cross sections for ions of the cerium isonuclear sequence. *Phys. Rev. A* **2009**, *80*, 033407. [CrossRef]

85. Pradhan, A.K.; Nahar, S.N.; Montenegro, M.; Yu, Y.; Hang, H.L.; Sur, C.; Mrozik, M.; Pitzer, R. Resonant X-Ray Enhancement of the Auger Effect in High-Z atoms, molecules, and Nanoparticles: Biomedical Applications. *J. Phys. Chem. A* **2009**, *113*, 12356–12363. [CrossRef] [PubMed]

86. Vinko, S.M.; Ciricosta, O.; Cho, B.I.; Engelhorn, K.; Chung, H.-K.; Brown, C.R.D.; Burian, T.; Chalupský, J.; Falcone, R.W.; Graves, C.; et al. Creation and diagnosis of a solid-density plasma with an X-ray free-electron laser. *Nature* **2012**, *482*, 59–62. [CrossRef] [PubMed]

87. Nahar, S.N.; Pradhan, A.K. K_α resonance fluorescence in Al, Ti, Cu and potential applications for X-ray sources. *J. Quant. Spectrosc. Radiat. Transf.* **2015**, *155*, 32–48. [CrossRef]

88. Nahar, S.N.; Shafique, B. Spectra of phosphorus ions for astrophysical modeling: P I–P XV. *Can. J. Phys.* **2024**, *in press*. [CrossRef]

89. Nahar, S.N. Theoretical spectra of lanthanides for kilonovae events: Ho I-III, Er I-IV, Tm I-V, Yb I-VI, Lu I-VII. *Atoms* 2024, *in press*.

90. Nahar, S.N.; Shafique, B. Collisional- and photo-excitations of Ca IV including strong 3.2 μm emission line. *Eur. Phys. J. D* **2023**, *77*, 45. [CrossRef]

91. Ankita, S.; Tauheed, A. Revised and extended analysis of the third spectrum of silver: Ag III. *J. Quant. Spectros. Rad. Transf.* **2018**, *217*, 130–154. [CrossRef]

92. Ankita, S.; Tauheed, A. Spectral analysis of triply ionized silver (Ag IV). *J. Quant. Spectros. Rad. Transf.* **2020**, *254*, 107193. [CrossRef]

93. Tauheed, A.; Rashid, A. Energy structure and radiative parameter calculations in the Re-like Pt IV, Au V and Hg VI spectra and preliminary line identifications in Hg VI. *J. Quant. Spectrosc. Radiat. Transf.* **2021**, *261*, 107435. [CrossRef]

94. Arya, N.K.; Tauheed, A. Energy levels, wavelengths and radiative rates for transitions in Hg-like Bismuth. *J. Quant. Spectros. Rad. Transf.* **2022**, *292*, 108353. [CrossRef]

95. Rashid, A.; Tauheed, A. Revised analysis of doubly ionized mercury: Hg III-3. *J. Quant. Spectrosc. Radiat. Transf.* **2019**, *233*, 119–133. [CrossRef]

96. Rashid, A.; Tauheed, A. Energy structure investigations in triply ionized mercury: Hg IV. *J. Quant. Spectrosc. Radiat. Transf.* **2021**, *270*, 107668. [CrossRef]

97. Hoy, K.; Nahar, S.N.; Pradhan, A.K. Biosignature Line Ratios of [P II] in Exoplanetary andNebular Environments. *Mon. Not. R. Astron. Soc. Lett.* **2023**, *521*, L48–L52. [CrossRef]